Electronic Supplementary Material (ESI) for Soft Matter.

Supporting Information for: Responsive Blends of Block Copolymers Stabilize the Hexagonally Perforated Lamellae Morphology

Samantha R. Nowak, Nikhil Tiwale, Gregory S. Doerk, Chang-Yong Nam, Charles T. Black,* Kevin G. Yager*

Center for Functional Nanomaterials, Brookhaven National Laboratory, Upton, New York 11973, United States

*email: ctblack@bnl.gov, kyager@bnl.gov

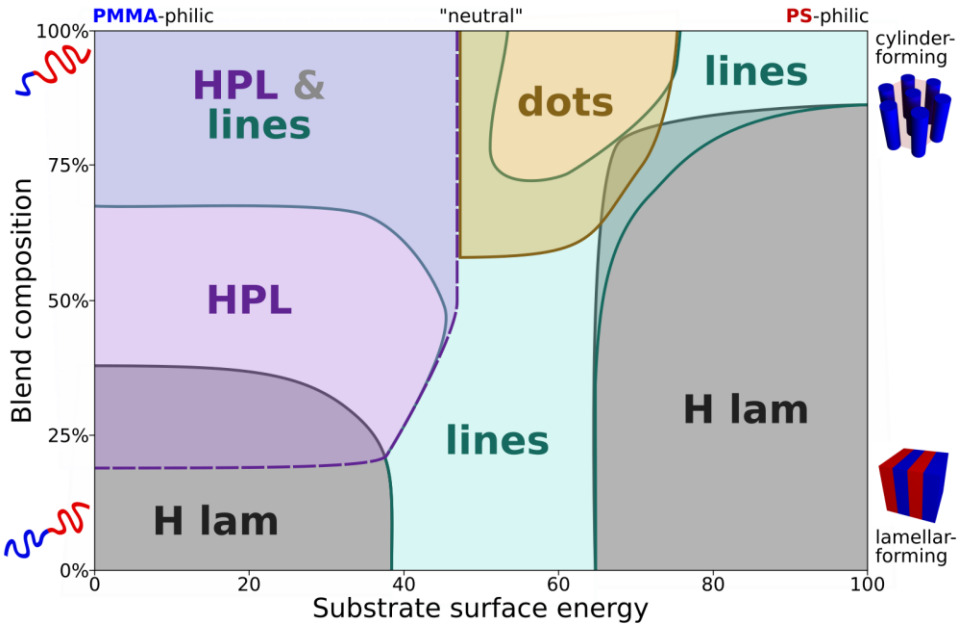

Figure S1: Morphology diagram showing the phases observed for blends of cylinder (C) and lamellar (L) materials ordered across a range of substrate surface energies. The ordering is inferred from the available SEM and GISAXS data. In several parts of the parameter space, coexistence of multiple phases is observed (denoted by overlap of the regions). The expected canonical BCP phases are observed, including horizontal lamellae (H lam), vertical lamellae (which appear as lines), vertical cylinders (dots), and horizontal cylinders (lines). Blending enables a continuous transformation from vertical lamellae into horizontal cylinders. The hexagonally perforated lamellar (HPL) phase is observed across a wide range of conditions. Blending influences the relative energy of phases. This enables broad ranges of coexisting phases (where blending stabilizes defects in both phases and brings their energies close to one another), but also generates a broad region where a pure HPL phase is observed (since blending stabilizes both the high-curvature perforations and the low-curvature sheets inherent to this morphology).

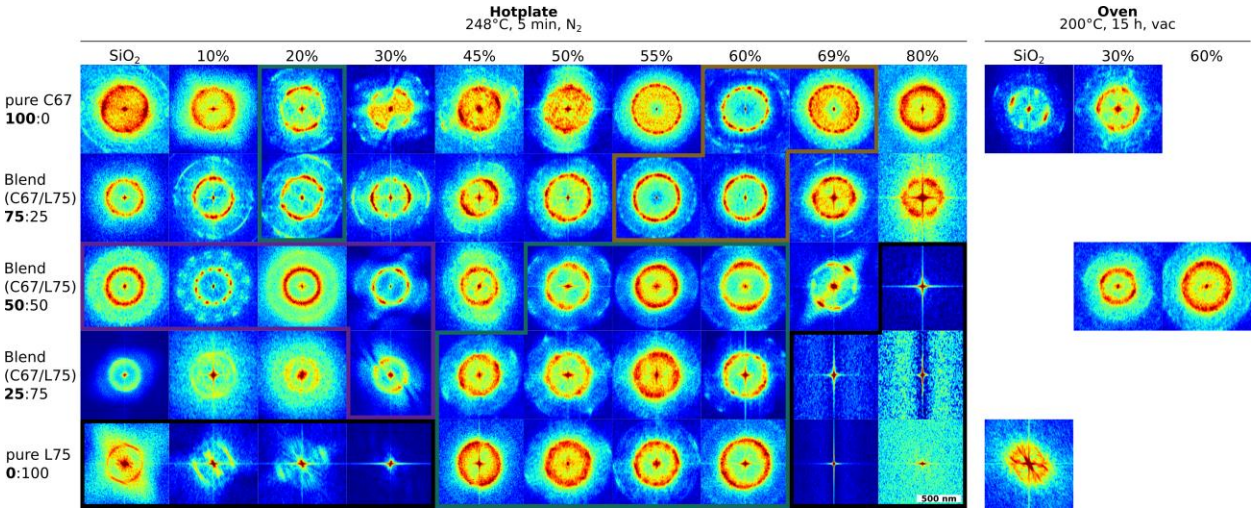

Figure S2: Fourier transforms (FFTs) of top-view SEM images for blend materials ordered across a range of substrates (denoted by the PS fraction of the PS-*r*-PMMA substrate brush). Results for hotplate annealing (in inert atmosphere) and vacuum oven annealing are compared.

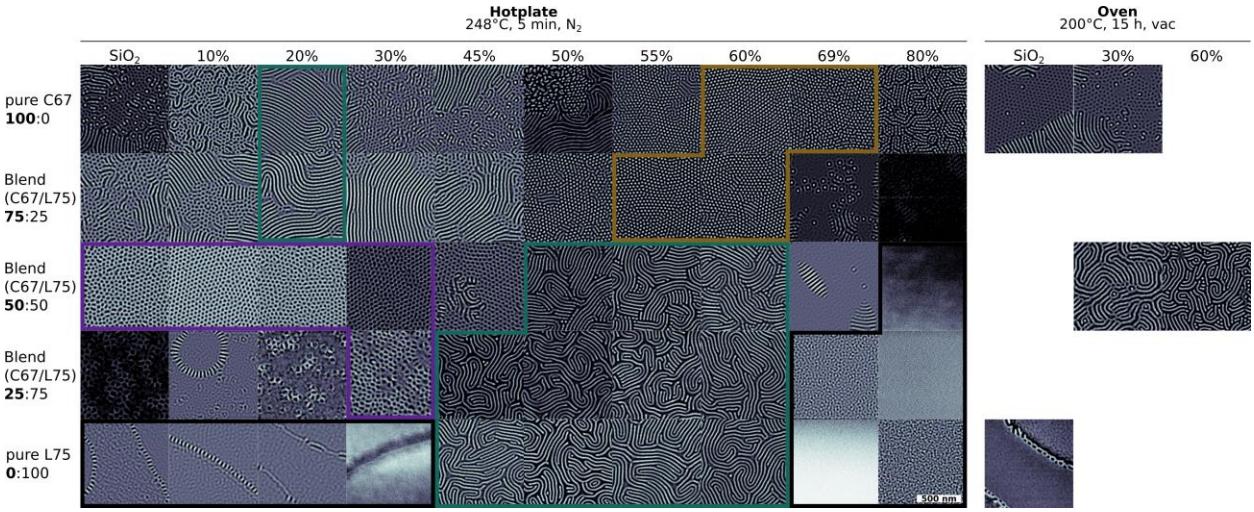

Figure S3: Fourier-filtered SEM images, obtained by rejecting Fourier components (both high- and low-frequency) away from the central peak associated with the BCP morphology. This representation highlights the structure of the morphology.

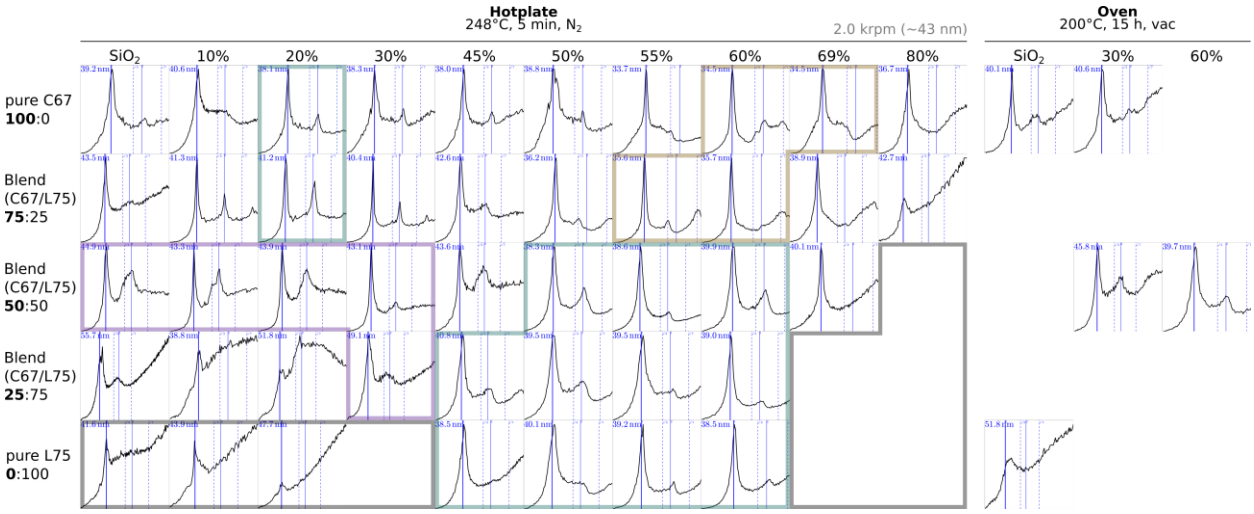

Figure S4: One-dimensional (1D) Fourier spectra (intensity vs. q) obtained by circular-average of the two-dimensional (2D) Fourier transforms (Figure S2) and multiplying by q^2 to renormalize. Each curve is fit using a Gaussian peak shape near the expected position of the primary morphological peak. The fit peak position (q_0) provides a measure of the repeat-spacing of the morphology ($L_0 = 2\pi/q_0$). The positions of higher-order peaks provide a means of evaluating the repeating lattice (for convenience, guiding lines are provided to denote the positions of $3^{½}$, 2, and $7^{½}$ times the fundamental peak position). The morphology repeat-spacing is responsive to substrate conditions, especially for blend materials. Notably, repeat-spacings of blends are not simply the average of the constituent pure materials, and may even exhibit structural spacing that exceeds either of the constituents. For instance, a 25:75 blend (C67:L75) ordering on a 30% PS substrate forms a defective HPL morphology with a repeat-spacing of ~49 nm, which is 1.3× the spacing of the pure components.

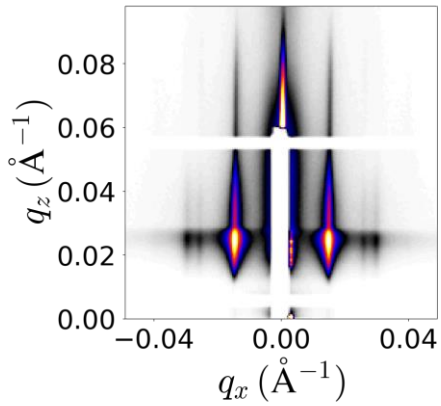

Figure S5: Representative grazing-incidence small-angle x-ray scattering (GISAXS) image. The presented data is a 43 nm thin film of a 50:50 blend of C67 and L75, cast on a 20% PS substrate. The grazing-incidence angle was 0.1°. The succession of peak positions along q_x is consistent with a hexagonal lattice, helping to confirm the formation of a horizontally-oriented hexagonally perforated lamellar (HPL) morphology through the depth of the film.

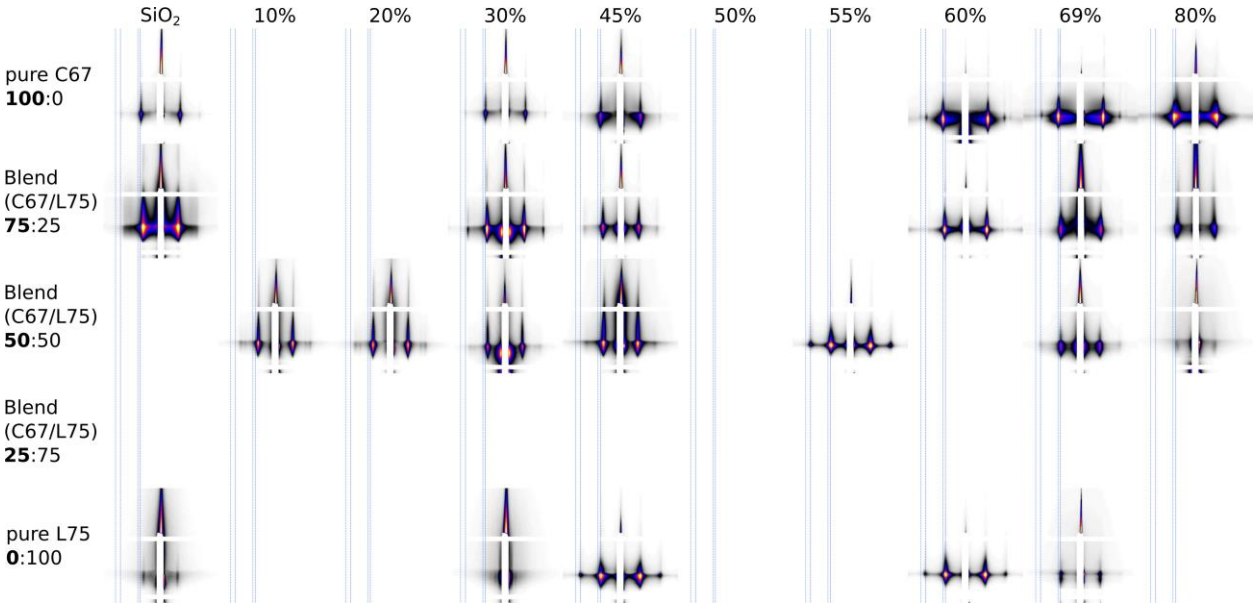

Figure S6: Grazing-incidence small-angle x-ray scattering (GISAXS) images for a range of BCP thin films (pure and blend materials) ordering on a range of substrates (percentage indicates PS content of PS-*r*-PMMA random brush). Each image spans a q-range of –0.049 to +0.049 Å^{-1} in the q_x direction, and 0.0 to 0.098 Å^{-1} in the q_z direction. The GISAXS results confirm the morphologies identified using SEM. The vertical lines are provided as a guide for the eye (lowest-q line aligned with the peak position for pure C67 ordering on 30% PS substrate), showing that the scattering peak positions shift substantially as a function of both blend ratio and substrate energy, confirming that the morphological repeat-spacing is responsive to these parameters. The response is most dramatic for the blend materials.

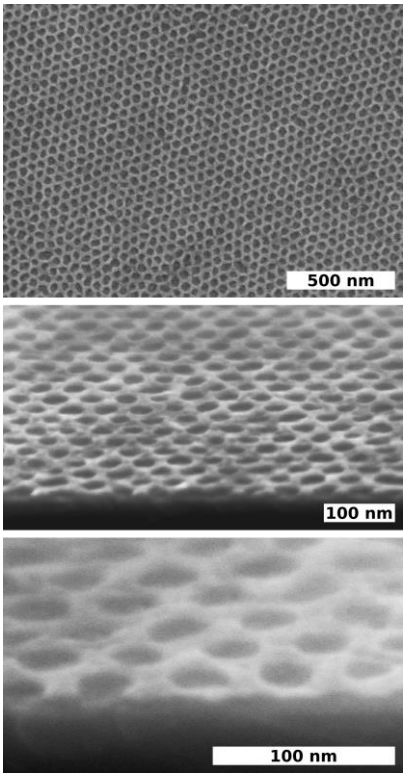

Figure S7: Scanning Electron Microscopy (SEM) images of a typical HPL phase, after infiltration synthesis to convert the PMMA into an inorganic replica, and plasma treatment to remove the PS matrix. Topview (top) and 70° tilt view (middle, bottom) images are shown for a 50:50 blend of C67 and L75, cast onto a 10% PS substrate.

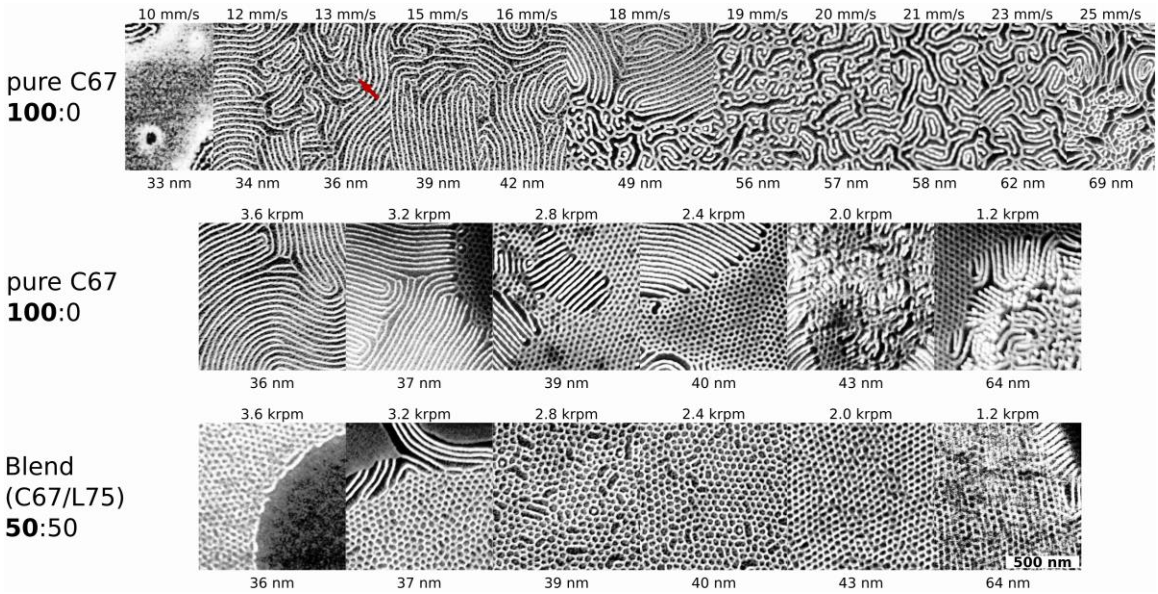

Figure S8: Thickness dependence of ordering for pure C67 and C67/L75 blends ordered on 30% PS substrates. A thickness gradient was created using flow-coating with an accelerating velocity profile (acceleration 9 mm/s^2 over ~50 mm; i.e. from 0 mm/s to 30 mm/s). Each image is labelled with the instantaneous velocity at that position (above image) and the corresponding local thickness (below image). These are compared to results for different thicknesses obtained using spin-coating (rotation speed noted above each image). Thickness clearly plays a role in selecting the morphology that arises. The blend material evidently forms a homogeneous HPL phase over a wider thickness range than the pure C67 material. The results for pure C67 obtained from flow-coating and spin-coating are somewhat different. Whereas spin-coated films form coexisting phases of HPL (along with horizontal cylinders) upon thermal annealing, the flow-coated films do not. There is weak evidence of HPL-like motifs appearing (e.g. red arrow), but no large grains of HPL arise. The difference may be due to the different evaporation rate associated with the two film formation methods, which correspondingly give rise to different latent states.

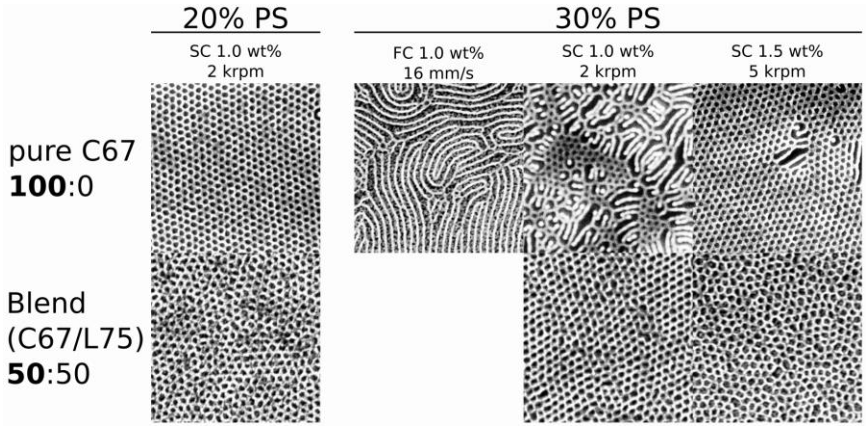

Figure S9: The evaporation rate of the film casting process influences the morphology that forms after thermal annealing. Different casting methods and casting parameters are used to give rise to the same nominal thickness (~42 nm for the results shown here). Both flow-coating (FC, velocity noted) and spin-coating (SC, rotation speed noted) are investigated. For spin-casting, one can achieve the same film thickness by varying both solution concentration and spin-speed. Although the final film thickness is identical, the evaporation rate will be larger when using high rotation speed. For pure C67, different morphologies arise (especially a different fraction of the HPL phase) depending on the casting method employed. This implies that the casting leaves a latent imprint in the film (the amount of residual solvent, the extent of early phase separation, weak chain alignment, etc.) which in turn influences the morphology that arises during thermal annealing. Faster evaporation rates give rise to more robust formation of the HPL phase. Appropriate selection of processing parameters can thus give rise to a high-quality HPL phase in pure C67 films (e.g. film formed using 1.0 wt%, 2 krpm, and cast on a 20% PS substrate). On the other hand, the C67/L75 blend is intrinsically responsive and stabilizes the HPL phase; as a result, it is easily formed using a broad range of conditions.

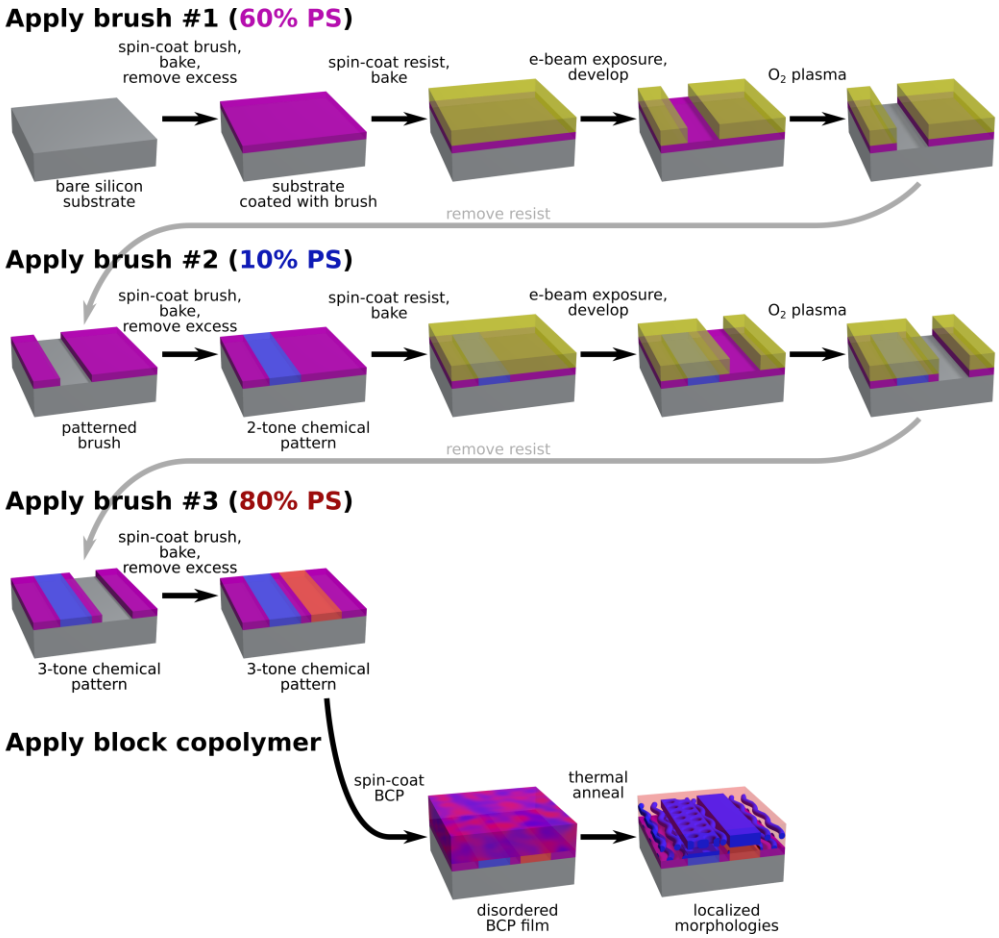

Figure S10: Detailed workflow for lithographic patterning used to yield a 3-tone chemical pattern. An initial brush (60% PS) is coated onto a silicon wafer. A layer of PMMA photoresist (yellow) is added, exposed using e-beam, and developed to remove resist in the exposed regions. Oxygen plasma treatment is used to remove the revealed brush, and thereby make the SiO_2 wafer surface (grey) available in the exposed areas. After removal of resist, the substrate is available for another iteration of the patterning process. The second brush (10% PS) is applied, forming a 2-tone chemical pattern that can be used to direct BCP assembly. For a 3-tone pattern, this substrate is subjected to the same workflow: application of resist, exposure, development, and plasma treatment; which again yields a substrate with SiO_2 regions available for brush attachment. After resist removal, the substrate (exhibiting regions of 60% PS, 10% PS, and bare SiO_2) is already a 3-tone chemical pattern. The SiO_2 regions can be converted into a different chemistry by attachment of a third brush (80% PS), to yield a 3-tone chemical pattern formed from 3 brushes. A BCP blend film (50:50 C67 and L75) is applied using spin-coating, and thermally annealed. The ordered morphological patterns that arise depend on the local surface chemistry. Thus, the multi-tone chemical patterning, combined with the responsive assembly of the blend, enable patterning of morphologies.

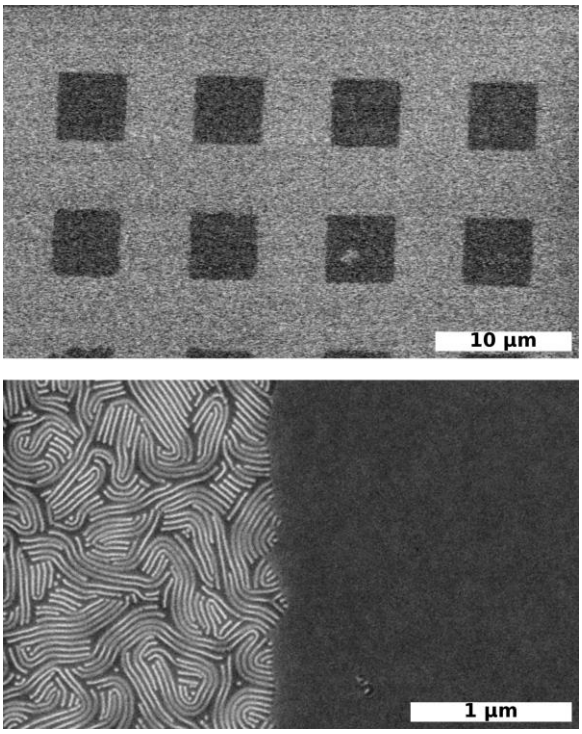

Figure S11: Example of morphological patterning. A BCP blend (50:50 C67 and L75) is ordered on a 2-tone chemical pattern consisting of squares (top). A zoomed-in view (bottom) shows a sharp interface between the two morphologies (horizontal cylinders and horizontal lamellae).

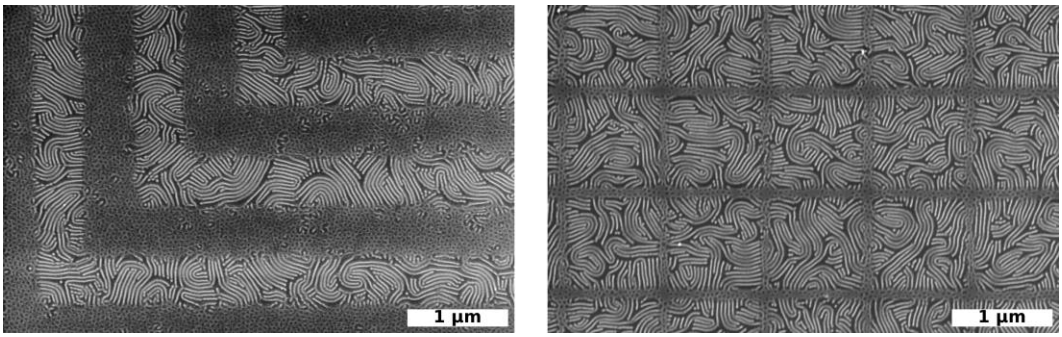

Figure S12: Example of morphological patterning. A BCP blend (50:50 C67 and L75) is ordered on various 2-tone chemical patterns. The distinct local surface chemistries give rise to different morphologies (horizontal cylinders and HPL).

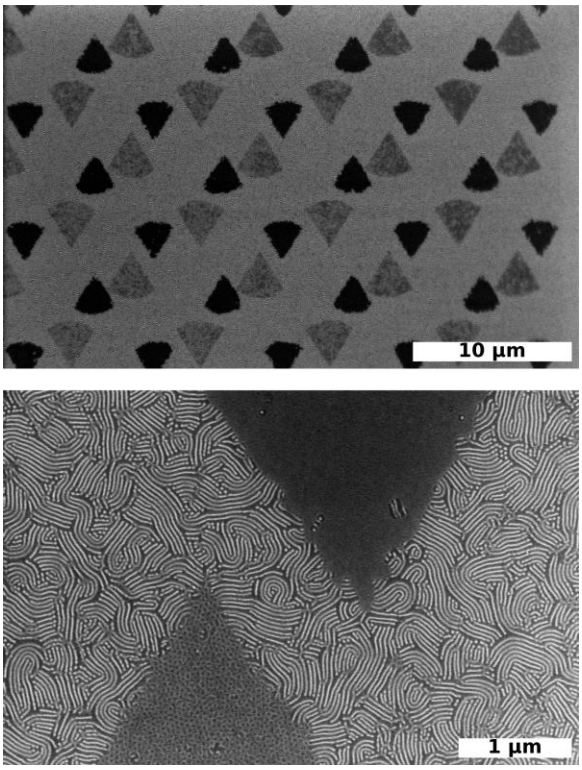

Figure S13: Example of morphological patterning. A BCP blend (50:50 C67 and L75) is ordered on a 3-tone chemical pattern. The distinct local surface chemistries give rise to different morphologies (horizontal cylinders, HPL, and horizontal lamellae).

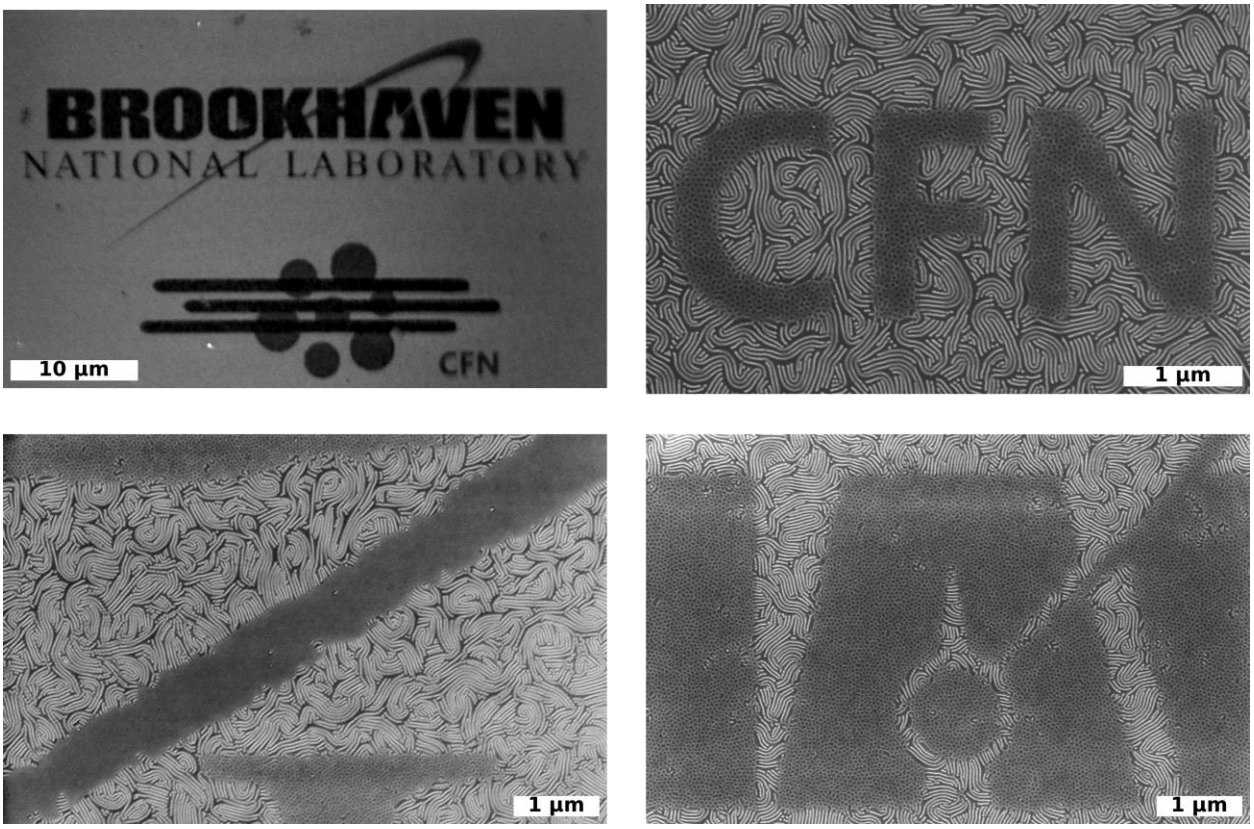

Figure S14: Example of arbitrary microscale patterns formed of different BCP morphologies. A BCP blend (50:50 C67 and L75) is ordered on multi-tone chemical patterns. The distinct local surface chemistries give rise to different morphologies (horizontal cylinders, HPL, and horizontal lamellae).